J. Plasma Physics (2013), vol. 79, part 2, pp. 143–152. © Cambridge University Press 2013
doi:10.1017/S0022377812000736

Laser wakefield compression and acceleration of externally injected electron bunches in guiding structures

N. E. ANDREEV[1,2], V. E. BARANOV[1], B. CROS[3], G. MAYNARD[3], P. MORA[4] and M. E. VEYSMAN[1]

[1]Joint Institute for High Temperatures of Russian Academy of Sciences, Moscow, Russia (andreev@ras.ru)
[2]Moscow Institute of Physics and Technology (State University), Moscow, Russia
[3]Laboratoire de Physique des Gaz et des Plasmas, CNRS-Universite Paris-Sud 11, Orsay, France
[4]Centre de Physique Theorique, CNRS, Ecole Polytechnique, Palaiseau Cedex, France

(Received 8 April 2012; revised 20 June 2012; accepted 10 July 2012; first published online 3 January 2013)

Abstract. For the considered scheme of the external electron bunch injection in front of a laser pulse, the influence of the nonlinear driving laser pulse dynamics and electron bunch self-action to the processes of electron bunch compression and acceleration in the laser wakefield is analyzed. Self-consistent modelling results confirm that the nonlinear laser pulse dynamics limits the bunch compression due to variations of the phase velocity of the wake. A growth of the injected bunch charge leads to some extent to an increase of the trapped and accelerated bunch charge and to decrease of the trapped bunch radius and emittance due to increased self-focusing bunch. The three-dimensional theoretical model is elaborated and used to describe the propagation of laser pulses in dielectric capillary waveguides under imperfect coupling and focusing conditions with broken cylindrical symmetry. The role of cone entrances to the cylindrical part of a capillary is analyzed, and it is demonstrated that matching cones can considerably increase the transmission of laser pulses through the capillary, but cannot mitigate the requirements on the precision of the laser pulse focusing into a capillary. In order to avoid a speckle structure and strong transverse gradients of the fields, which can prevent the process of regular electron bunch acceleration, one has to ensure a small laser angle of incidence into the capillary not exceeding 1 mrad.

1. Introduction

One of the most attractive applications of short intense laser pulses is the laser wakefield acceleration (LWFA) of electrons (Tajima and Dawson 1979; Gorbunov and Kirsanov 1987; Esarey et al. 1996, 2009). A few orders of magnitude of higher acceleration rate (than in traditional high-frequency accelerators), and so small possible sizes of the laser wakefield accelerator are the main advantages of this device. At the same time, a short-scale inhomogeneity of accelerating and focusing wakefields, which can prevent monoenergetic acceleration, and also necessity to propagate an intense laser pulse over a long enough distances to accelerate electrons to high energies are the problems that should be solved on the way of realization of LWFA of high quality electron bunches with low energy spread and emittance.

In the so-called 'standard LWFA' considered here, when moderately nonlinear laser wakefields are generated in a rarefied plasma by the laser pulse of weakly relativistic intensity ($\geqslant 10^{18}$ W/cm^2 for the one micron laser wavelength), the laser should propagate over many Reyleigh lengths for efficient acceleration of electrons to GeV energies that usually needs the usage of some guiding structures, such as plasma channels or/and gas-filled capillaries, to overcome laser pulse diffraction (Zigler et al. 1996; Spence and Hooker 2000; Courtois et al. 2001; Wojda et al. 2009; Abuazoum et al. 2012).

The quality of accelerated electron bunches (energy spread, emittance, bunch length, and charge) is of crucial importance for many applications (Wiggins et al. 2010) and is determined substantially by the method of electron bunch injection into the accelerating wakefields (Esarey et al. 2009). One of the possible approaches to produce stable and controllable acceleration of electrons is based on the external injection of electron bunches into the wakefield generated in a moderately nonlinear regime. For monoenergetic, low-emittance acceleration of electron bunches externally injected into the wakefield, the bunch sizes have to be much shorter than the wavelength of the accelerating wakefield, which is typically of the order of hundred microns for one micron driving laser (see, e.g. Andreev and Kuznetsov 2003). At the same time, a few tens of microns electron bunch length is near the limit of current RF injectors. That is why the electron bunch compression in the wakefield before accelerating stage is necessary for monoenergetic

https://doi.org/10.1017/S0022377812000736 Published online by Cambridge University Press

acceleration. The maximal bunch compression can be achieved when the electrons are injected in front of the laser pulse in the region of zero fields (see Andreev and Kuznetsov 2003; Andreev et al. 2011b and references therein). In this paper, the transverse dynamics and loading effect of the electron bunch injected in front of the laser pulse, together with the laser pulse dynamics in its propagation in the plasma channel, are analyzed and limitations to the final bunch charge, energy spread, and compressed sizes are discussed extending our previous analysis (Andreev et al. 2011a).

In the case of LWFA in gas-filled capillaries, the violation of cylindrical symmetry and non-perfect focusing of laser at the capillary entrance can lead to substantial distortions of the laser pulse transmission and intensity distribution, and so to the non-regular wakefield structure generated by the laser propagating in capillary (Veysman et al. 2010). Therefore, a special analysis of the influence of possible non-perfect focusing of laser pulse at the capillary entrance on the dynamics of laser pulse propagation inside a capillary and on the structure of laser fields under conditions of real experiments is required. In this paper, the dynamics of laser field is studied for the case of small non-zero angles of incidence of laser pulses on the capillary entrance. Possible advantages of the use of capillaries with cone entrances are also demonstrated.

The paper is organized as follows: The trapping and compression of electron bunches injected in front of the laser pulse propagating in a plasma channel are analyzed in Sec. 2; the dependencies of the accelerated bunch parameters on the initial bunch charge and laser intensity are presented in Sec. 3; laser propagation in a capillary waveguide at non-perfect focusing and broken symmetry is described in Sec. 4; and conclusion is given in Sec. 5.

2. Dynamics of finite-charge bunch compression in plasma channel

In this and the following sections, the adjusted plasma channel with parabolically increasing plasma density from the axis is used as a guiding structure to compensate laser pulse diffraction (for the laser pulses with power less than the critical one for relativistic self-focusing) and to provide a long-distance laser propagation over many Reyleigh lengths that is necessary for efficient acceleration of electron bunches to high energies. The electron bunch externally injected along the plasma channel axis propagates initially in front of the laser pulse focused also to the plasma channel along the channel axis. In order the bunch can be overtaken by the laser pulse and then trapped and accelerated by the laser wakefield, the initial bunch velocity should be smaller than the group velocity of the laser pulse (determined mainly by the electron plasma density). The scheme of electron bunch injection in front of the laser pulse can provide very high bunch compression. This effect of electron bunch compression is caused by relativistic electron dynamics in the process of particle 'reflection' from the potential wall (changing of the electron velocity direction in relation to the wake wave) during bunch trapping into the wakefield. The compression ratio depends on the injection energy, E_{inj}, and phase velocity of the accelerating wakefield (Andreev and Kuznetsov 2003; Andreev et al. 2011a,b):

$$L_b/L_{b0} \approx E_{\mathrm{inj}}^2/(\gamma_{\mathrm{ph}} m^2 c^4), \tag{2.1}$$

where L_b and L_{b0} are the compressed and initial root mean square (rms) lengths of the bunch, m and c are the electron mass at rest and speed of light, $\gamma_{\mathrm{ph}} = (1 - V_{\mathrm{ph}}^2/c^2)^{-1/2}$ is the phase gamma-factor corresponding to the phase velocity of the wake V_{ph}. In the moderately nonlinear regime, the wake phase velocity is close with the group velocity of the laser pulse, and so for a wide driving laser pulse propagating in a rarefied plasma with waist radius $r_0 \gg 1/k_p = c/\omega_p$, phase velocity of the wake wave is determined by the plasma density, $\gamma_{\mathrm{ph}} \cong \omega_0/\omega_p \gg 1$, where ω_0 is the laser frequency, $\omega_p = \sqrt{4\pi e^2 n_0/m}$ is the electron plasma frequency, and e, m, and n_0 are the electron charge, mass, and background electron plasma density respectively. The important condition for trapping of the bunch injected in front of the laser pulse (with energy less than the resonant one $E_{\mathrm{inj}} < \gamma_{\mathrm{ph}} mc^2$) is the potential depth of the wakefield potential in the trapping point, which should be in the focusing phase of the wakefield:

$$-\triangle\varphi = E_{\mathrm{inj}}/mc^2 - \left[\left(1 - \gamma_{\mathrm{ph}}^{-2}\right)\left(E_{\mathrm{inj}}^2/m^2c^4 - 1\right)\right]^{1/2}, \tag{2.2}$$

where $\varphi = e\delta\Phi/mc^2$ is the dimensionless wakefield potential. This condition can be satisfied if the wake wave is nonlinear, or/and is excited in the plasma channel, where the accelerating and focusing phases of the wave are overlapped deeper than in the linear plasma wave (Andreev et al. 1997).

The one-dimensional (1D) estimation (2.1) was obtained under assumption of the constant phase velocity during the bunch trapping and compression, and also neglecting self-action of bunch electrons (loading effect) and their ponderomotive repulsion by laser pulse. We have analyzed all these effects in self-consistent 3D modelling of the laser and bunch dynamics by the code LAPLAC (Andreev and Kuznetsov 2008). The code describes the nonlinear laser pulse dynamics and wakefield generation using cold hydrodynamics for background plasma electrons (with immobile ions) in cylindrical symmetry together with the relativistic 3D dynamics of bunch electrons described by the particle-in-cell (PIC) method.

The initially Gaussian in space and time laser pulse with the waist radius $r_0 = 2.34\ k_p^{-1}$ and pulse duration $\tau_L = 0.5\ \omega_p^{-1}$ was focused into the parabolic plasma channel with radius adjusted to the laser focal spot by the linear matching condition (Sprangle and Esarey 1992; Andreev et al. 1995): $R_{\mathrm{ch}} = k_p r_0^2/2$, where ω_p

https://doi.org/10.1017/S0022377812000736 Published online by Cambridge University Press

Table 1. Final characteristics of accelerated electron bunches at different amplitudes of the driving laser pulse.

a_0	1.0	1.2	1.4	1.4	1.5
Initial charge $q_{\rm inj}$ (pC)	2.5	2.5	2.5	10	2.5
Initial rms length, L_{b0} (μm)			47		
Initial rms radius, R_{b0} (μm)			33		
Compressed rms length L_b, μm	1.28	1.18	1.05	1.63	0.99
Compressed rms radius, R_b (μm)	2.01	2.08	2.06	1.61	2.14
Trapped charge, q (pC)	0.68	0.58	0.49	2.76	0.47
Final energy, E (MeV)	1069	1445	1903	1929	2180
Energy spread, $\triangle E/E$ (%)	3.4	3.6	3.9	5.5	4.9
Normalized emittance, ϵ_n (mm × mrad)	11.3	16.1	18.9	12.6	21.6

and $k_p = \omega_p/c$ are determined by the plasma density at the channel axis $n_0(r = 0)$. The electron plasma density at the channel axis is chosen so that the linear phase gamma-factor equals to $\gamma_{\rm ph} = \omega_0/\omega_p = 100$. For one micron wave length laser, these dimensionless parameters correspond to a plasma density, $n_0(r = 0) = 1.12 \times 10^{17}$ cm^{-3}, waist radius, $r_0 = 37$ μm, laser pulse duration, and $\tau_{FWHM} = 31$ fs. The normalized amplitude of the laser, $a_0 = 1.5$ for Fig. 1 and 1.4 for calculations presented in Figs. 2–6 that provides bunch trapping (in accordance with (2.2)) for injected energies exceeding 1.5 MeV. For these two laser amplitudes the laser intensities, $I_L = (2.69 \text{ and } 3.08) \times 10^{18}$ W/cm^2, energies 1.96 and 2.25 J, and power, $P_L = 59$ and 68 TW, respectively, which corresponds to the ratios of power to the critical one for relativistic self-focusing $P_L/P_{\rm cr} = 0.35$ and 0.40.

Electron bunches were injected in front of the laser pulse along the channel axis with comparatively low energies, $E_{\rm inj} = 3 \div 10$ MeV, have zero energy spread, and different bunch charges: 2.5 and 10 pC. At the channel entrance the bunches are described by a random distribution of particles with Gaussian density profiles in both transverse and longitudinal directions ($\xi = k_p(z - ct)$ and $\rho = k_p r$ are the dimensionless variables):

$$n_b(\xi, \rho, z = 0) = n_{b0} \exp\left(-(\xi - \xi_{\rm inj})^2/2(k_p\sigma_z)^2 - \rho^2/2(k_p\sigma_\perp)^2\right) \quad (2.3)$$

with $k_p\sigma_\perp = k_p\sigma_z = 1.48$ that corresponds to rms bunch length, $L_{b0} = 2\sigma_z = 47$ μm. For most of the runs (see Table 1) the imposed random Gaussian distribution of particles over transverse momentum corresponds to an initial normalized radial emittance $\epsilon_{N,r} = 4\, R_{b0}\sigma_{P_r/mc} = 1$ mm × mrad (i.e. $\epsilon_{N,x} = \epsilon_{N,y} = 1/\sqrt{2}$ mm × mrad) at the rms bunch radius $R_{b0} = \sqrt{2}\sigma_\perp = 33$ μm, and $\sigma_\perp = R_{b0}/\sqrt{2} = 23$ μm.

Figure 1 illustrates 1D prediction of the longitudinal bunch compression (2.1) by a solid line, and also the results of modelling for different electron bunch parameters. As it was shown earlier (Andreev et al. 2011a), for the prescribed laser pulse (without nonlinear laser dynamics, and so for the constant group laser and phase wakefield velocities) and neglecting loading

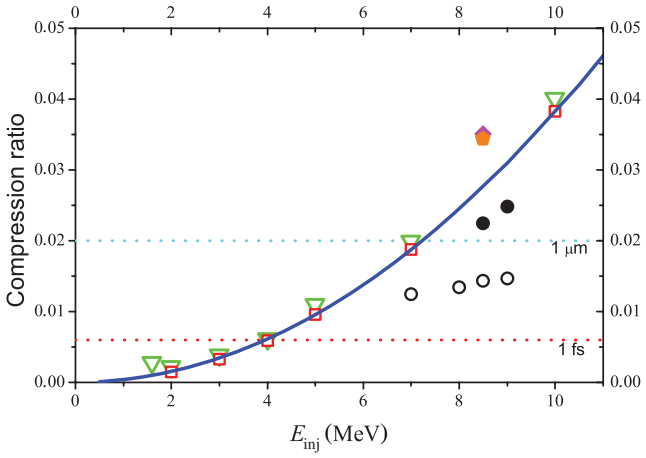


Figure 1. (Colour online) Compression ratio of the electron bunch as a function of the injection energy for $\gamma_{\rm ph} = 100$ and initial bunch length $L_{b0} = 47$ μm. Solid line is the analytical prediction (2.1). Open symbols are 3D modelling results for the prescribed laser pulse (without nonlinear laser dynamics) with different injected bunch radii R_{b0}: triangles and squares show results without loading effect, $R_{b0} = 2$ μm; squares – without influence of ponderomotive force; circles – with loading effect, $R_{b0} = 33$ μm, emittance of injected bunch is 1 mm × mrad and charge $q_{\rm inj} = 2.5$ pC. Solid symbols indicate fully self-consistent modelling (with loading effect and laser pulse dynamics), emittance of injected bunch is 1 mm × mrad; circles – $R_{b0} = 33$ μm, injected charge $q_{\rm inj} = 2.5$ pC; rhombus – $R_{b0} = 33$ μm, $q_{\rm inj} = 10$ pC; pentahedrons – $R_{b0} = 45$ μm, $q_{\rm inj} = 10$ pC. Two horizontal dotted lines indicate the values of compression ratio, for which the bunch length L_b reaches 1 μm size and 1 fs duration ($= L_b/c$) respectively for the initial bunch length $L_{b0} = 47$ μm.

effect for small radius electron bunches, the modelling results confirm analytical prediction (2.1), especially when the influence of the ponderomotive laser force to the bunch electrons was neglected (see open squares and triangles in Fig. 1). At the same time, the self-consistent 3D electron bunch dynamics can lead to even higher longitudinal bunch compression than predicted by one-dimensional theory for test bunch particles (see circle points for injection energies in excess of 5 MeV). Comparison of modelling results indicated in Fig. 1 by open and solid circles shows that the nonlinear laser pulse dynamics (which influences the phase of generated wakefields) limits the bunch compression due to variations of the phase velocity of the wake.

Figures 2 to 5 demonstrate the longitudinal and transverse electron bunch dynamics under the action of self-generated wakefields just before the laser pulse overtakes the bunch (at the bunch propagation distance in laboratory frame $z \equiv L_{\rm acc} = 0.038\, L_{\rm ph}$, where $L_{\rm ph} = 2\pi\gamma_{\rm ph}^2 k_p^{-1}$ is the dephasing length). Substantial energy modulation of bunch electrons shown in Fig. 2, together with the transverse bunch self-focusing (lens effect) illustrated in Fig. 3, lead to pronounced electron bunch density redistributions in both longitudinal and transverse directions, as shown in Figs. 4 and 5. The phase space in Fig. 2 illustrates the influence of longitudinal self-generated wakefield, which accelerate electrons at the tail

https://doi.org/10.1017/S0022377812000736 Published online by Cambridge University Press

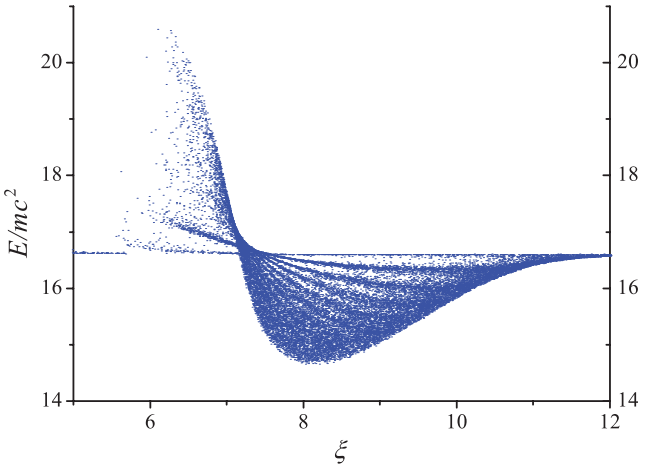


Figure 2. (Colour online) Distribution in the phase space $(E(\xi)/mc^2, \xi)$ at $L_{acc}/L_{ph} = 0.038$ of initially mono-energetic electron bunch injected in front of the laser pulse with energy $E_{inj} = 8.5$ MeV, initial charge $q_{inj} = 2.5$ pC, and Gaussian profile with initial rms bunch length $L_{b0} = 47$ μm ($k_p L_{b0} = 2.95$), initial rms bunch radius $R_{b0} = 33$ μm ($k_p L_{b0} = 2.07$), and initial normalized emittance $\epsilon_n = 1$ mm × mrad.

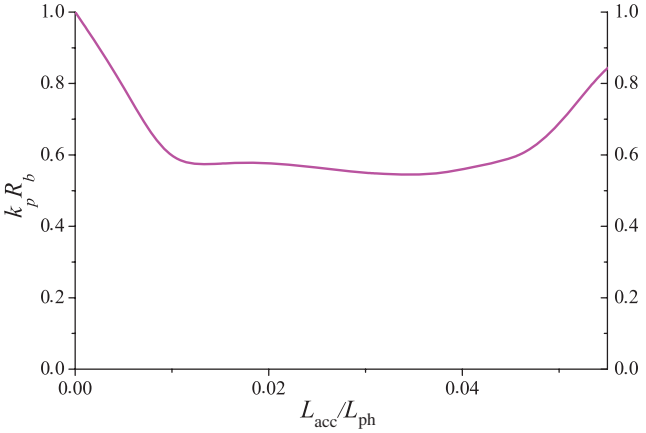


Figure 3. (Colour online) The rms radius of trapped and accelerated in sequel electrons as a function of normalized length of the bunch propagation L_{acc}/L_{ph}. Parameters of the laser, plasma, and injected electron bunch are the same as in Fig. 2.

of the bunch and decelerate head particles. At the same time, self-generated focusing forces lead to betatron-like variations of the bunch radius shown in Fig. 3. The characteristic length, which the bunch should propagate in plasma for radial contraction, can be estimated from the time which is necessary for a bunch electron (with energy E_{inj} located at the half of the bunch radius) in order to reach the axis under the action of self-generated focusing force (Andreev and Kuznetsov 2008):

$$z_f \approx \frac{\pi c}{\omega_p}\sqrt{\frac{E_{inj} n_0}{2mc^2 n_b}} \tag{2.4}$$

that gives $z_f \approx 1.3$ cm in accordance with the value $z \approx 1.4$ cm obtained in simulations (corresponds to $z = L_{acc} = 0.012\ L_{ph}$ in Fig. 3). The normalized bunch

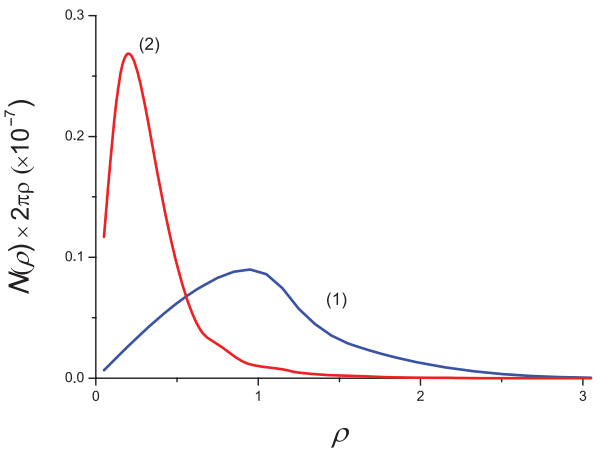


Figure 4. (Colour online) Integrated over ξ normalized radial density distribution of trapped and accelerated in sequel electrons $2\pi\rho N(\rho, z)$ determined by (2.5): blue line (1) is for injected Gaussian density profile at z =0, and red line (2) is the bunch density just in front of the laser pulse at $z = L_{acc} = 0.038 L_{ph}$. Parameters are the same as in Fig. 2.

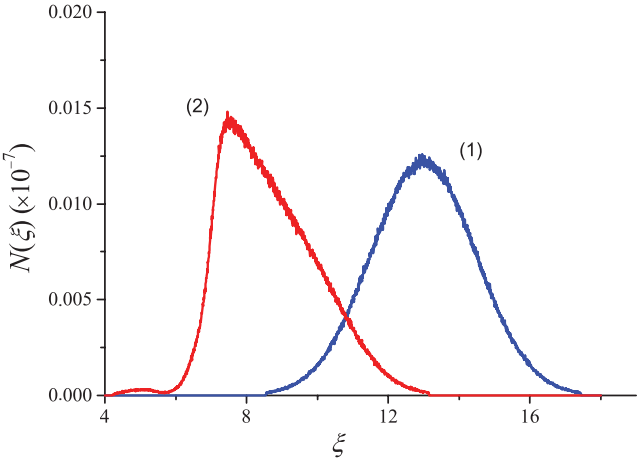


Figure 5. (Colour online) Normalized electron bunch density integrated over the radius, $N(\xi, z)$ (2.6): blue line (1) illustrates injected Gaussian density profile, and red line (2) is the bunch density just in front of the laser pulse at $z = L_{acc}/L_{ph} = 0.038$. Parameters are the same as in Figs. 2–4.

density integrated over ξ

$$N(\rho, z) = \frac{1}{n_0}\int_0^\infty n_b(\xi, \rho, z) d\xi \tag{2.5}$$

illustrated in Fig. 4 for the injected bunch (z =0, blue line (1)), and also after propagation in plasma the distance $z = L_{acc} = 0.038\ L_{ph}$ (just before colliding with the laser pulse, red line (2)), demonstrates reduction of rms bunch radius during propagation in front of the laser. For Figs. 3 and 4 only that bunch electrons were taken into account which in the sequel were trapped and accelerated in the wakefield.

The normalized bunch density integrated over the radius

$$N(\xi, z) = \frac{2\pi}{n_0}\int_0^\infty n_b(\xi, \rho, z)\rho d\rho \tag{2.6}$$

https://doi.org/10.1017/S0022377812000736 Published online by Cambridge University Press

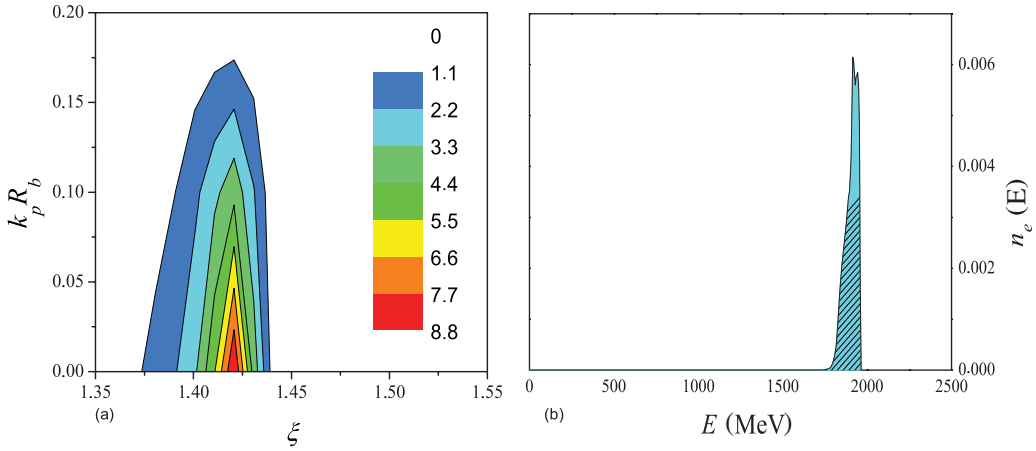


Figure 6. (Colour online) Final characteristics at the end of accelerating stage ($L_{acc}/L_{ph} = 0.33$): (a) spatial distribution of the normalized electron bunch density, $n_b(\xi, \rho, z = L_{acc})/n_0$, and (b) the bunch energy spectrum. Parameters of the modelling are the same as in Figs. 2–4.

shown in Fig. 5 for the injected bunch (z =0, blue line (1)), and also just before colliding with the laser pulse, red line (2), illustrates some shortening of the bunch due to density redistribution as a result of bunch energy modulation and radial focusing in the self-generated wakefield. These processes can be responsible for the more efficient compression of the bunch in its trapping into the laser wakefield in comparison with the simplified 1D prediction (2.1). This effect, determined by the bunch self-action, strongly depends on the bunch charge and energy as shown in Fig. 1.

3. Electron bunch acceleration in laser wakefields: modelling results

Acceleration of compressed electron bunches over the whole region, where accelerating and focusing phases of the wakefields overlap, was modelled for the above indicated injected bunch parameters: energy of injection, $E_{inj} = 8.5$ MeV, initial emittance is 1 mm × mrad, characteristic longitudinal and transverse sizes of the injected bunch with Gaussian density profile are $\sigma_z = \sigma_\perp = 23.5$ μm (that correspond to rms length and radius $L_{b0} = 2\sigma_z = 47$ μm and $R_{b0} = \sqrt{2}\sigma_\perp = 33$ μm). Table 1 presents the final characteristics of electron bunches injected with different total charges, $q_{inj} = 2.5$ and 10 pC, and accelerated in the wakefields generated by the laser pulses of different intensities with $a_0 = 1.0 - 1.5$ and all other parameters being the same as indicated in Sec. 2.

Due to reduction of the laser pulse group velocity (and so the phase velocity of the wakefield) caused by the finite pulse spot size (Schroeder et al. 2011), and also by the nonlinear laser pulse dynamics (Andreev and Kuznetsov 2008), the total length of acceleration for the discussed parameters is shorter than the one predicted by the linear dephasing length and equals to $L_{acc} = 0.33\ L_{ph}$, where $L_{ph} = \gamma_{ph}^2 \lambda_p$ is determined by the linear 1D expression of $\gamma_{ph} = \omega_0/\omega_p = 100$. This accelerating length is about 0.67 of the 'effective' dephasing length determined by the nonlinear modified gamma-factor, $\bar{\gamma}_{ph} \approx 70$, that was observed in the self-consistent modelling. Note that the length, $L_{acc} = 0.67\ \lambda_p \bar{\gamma}_{ph}^2$ corresponds to the motion (in the co-moving frame) of an electron from the small negative values of the wakefield potential (trapping point) to the potential maximum (end of acceleration). So the maximum length of acceleration, $L_{acc} = 0.33\ L_{ph}$ for the discussed parameters, determined by the real phase velocity of the wake, depends mainly on the reduced group velocity of the laser pulse that depends on the laser spot size and the laser field amplitude as a result of the nonlinear laser pulse dynamics. Figure 6 shows the final characteristics of accelerated bunch at the end of the accelerating phase, $L_{acc}/L_{ph} = 0.33$, for $a_0 = 1.4$ and $q_{inj} = 2.5$ pC: spatial distribution of the electron bunch density (Fig. 6(a)) and the bunch energy spectrum (Fig. 6(b)).

As it is clear from Table 1, an increase of the laser pulse intensity, and so generated wakefield amplitude, leads to the evident increase of the final energy of accelerated electrons. At the same time, due to the increased ponderomotive repulsing of electrons while the bunch travels through the laser pulse, increasing of the laser intensity is accompanied by the growth of the bunch emittance and energy spread with approximately constant compressed bunch radius and length. A growth of the injected bunch charge leads, to some extent, to an increase of the trapped and accelerated bunch charge and to decrease of the trapped bunch radius and emittance due to increased bunch self-focusing.

4. Laser propagation in capillary waveguide at non-perfect focusing

When a capillary tube is used as a guiding structure for a long-distance laser wakefield generation, the violation of cylindrical symmetry and non-perfect focusing of laser at the capillary entrance can lead to substantial distortions

https://doi.org/10.1017/S0022377812000736 Published online by Cambridge University Press

of laser pulse transmission and intensity distribution, and so to the non-regular wakefield structure generated by the laser propagating in capillary (Veysman et al. 2010). Under the real conditions of experiments with high-intensity laser pulses, the broken symmetry of the laser pulse intensity distribution, and also displacements of the laser from capillary axis (point stability and non-perfect alignment), can lead to the ablation of capillary entrance and walls, and so to the capillary damage. An improvement of the laser pulse coupling to a capillary can be achieved by using the cone entrance (Andreev et al. 2008).

To describe the laser pulse propagation in a capillary with variable radius, $R(z)$, namely a capillary with cone entrance, Maxwell equations with proper boundary conditions at the capillary entrance, $z = 0$, and at the capillary wall, $r = R(z)$, were solved for the angular harmonics of complex amplitudes of the fields, slowly varying over the laser period $2\pi\omega_0^{-1}$ and wavelength λ_0 (Veysman et al. 2012). The capillary is assumed to be a tube with slowly varying inner radius, $R = R(z)$, so that the local angle $\alpha \equiv |\partial R/\partial z| \ll 1$; the permittivity of capillary walls and the permittivity of the medium inside the capillary are assumed to be constant in space and time, $\varepsilon(r \geqslant R) = \varepsilon_w$, $\varepsilon(r < R) = \varepsilon_c$, $|1 - \varepsilon_c| \ll 1$; the axis OZ coincides with the capillary axis, while the laser pulse direction of propagation at the capillary entrance can be inclined from the capillary axis on some angle, θ_{inc}, and the laser focusing point can be displaced from the capillary axis, $r = 0$ on some value $\delta\boldsymbol{r}$. Here and below, cylindrical coordinates r, ϕ with the axis OZ are used and all equations are written down in dimensionless variables $\xi = k_0(z - ct)$, $\zeta = k_0 z$, $\rho = k_0 r$, where $k_0 = \omega_0/c$ and $\omega_0 = 2\pi c/\lambda_0$.

In the step-like approximation of a slowly variable radius, $R(z)$, a capillary with variable radius and length L_{cap} is replaced by a set of cylinders of lengths $h_j = z_j - z_{j-1}$, $j = 1, 2 \ldots j_{\max}$, $z_0 = 0$, $z_{j_{\max}} = L_{\text{cap}}$, with constant radii $R_j = R(z_{j-1})$. The solution to wave equations for laser fields at each interval $[z_{j-1}; z_j]$ can be obtained in terms of angular and radial modes of electromagnetic fields in the cylinder with radius R_j and length h_j. In this case the slowly varying normalized complex amplitudes $\boldsymbol{E}^j$ and $\boldsymbol{B}^j$ of laser fields $\widetilde{\boldsymbol{E}}^j = 1/2 A_{\max}\boldsymbol{E}^j e^{i\xi} + \text{c.c.}$ and $\widetilde{\boldsymbol{B}}^j = 1/2 A_{\max}\boldsymbol{B}^j e^{i\xi} + \text{c.c.}$ (where $A_{\max} \equiv \sqrt{8\pi I_0/c}$ is the maximum amplitude of the field at capillary entrance, and I_0 is the peak intensity of laser radiation in vacuum at the capillary entrance) in each jth interval can be described as follows:

$$\begin{Bmatrix} \boldsymbol{E} \\ \boldsymbol{B} \end{Bmatrix}^j = \sum_{l=-L}^{L} e^{il\phi} \sum_{\sigma=\pm 1} \sum_n \widetilde{\mathfrak{C}}^j_{l\sigma n}(\xi, \zeta) \begin{Bmatrix} \boldsymbol{E}_{l\sigma n}(\rho) \\ \boldsymbol{B}_{l\sigma n}(\rho) \end{Bmatrix}^j, \quad (4.1)$$

where $\boldsymbol{E}^j_{l\sigma n}$ and $\boldsymbol{B}^j_{l\sigma n}$ are the radial modes of electromagnetic fields inside the capillary, whose components are given by equations [1]

$$\begin{Bmatrix} E_z \\ B_z \end{Bmatrix}^j_{0\sigma n} = \mathrm{k}^j_{\perp 0\sigma n} J_0(y^j_{0-\sigma n}) \frac{1}{2} \begin{Bmatrix} i(1-\sigma) \\ 1+\sigma \end{Bmatrix},$$
$$\begin{Bmatrix} E_\phi \\ B_\phi \end{Bmatrix}^j_{0\sigma n} = J_1(y^j_{0-\sigma n}) \frac{1}{2} \begin{Bmatrix} i(1+\sigma) \\ 1-\sigma \end{Bmatrix}, \quad (4.2)$$

$$\begin{Bmatrix} E_z \\ B_z \end{Bmatrix}^j_{l\neq 0,\sigma n} = -\mathrm{k}^j_{\perp l\sigma n} \begin{Bmatrix} i\sigma + \mu^- u^2_{l-\sigma,n}/(l\mathscr{R}_j) \\ 1 \end{Bmatrix} J_l(y^j_{l\sigma n}); \quad (4.3)$$

$$\begin{Bmatrix} E_\phi \\ B_\phi \end{Bmatrix}^j_{l\neq 0,\sigma n} = \begin{Bmatrix} i\sigma \\ 1 \end{Bmatrix} J_{l-\sigma}(y^j_{l\sigma n}) + \mu^- u_{l-\sigma,n} \begin{Bmatrix} J_l(y^j_{l\sigma n})/\rho \\ -i\dfrac{u_{l-\sigma,n}}{l\mathscr{R}_j} \dfrac{\partial J_{l-\sigma}(y^j_{l\sigma n})}{\partial y^j_{l\sigma n}} \end{Bmatrix}, \quad (4.4)$$

$$E^j_{r,l\sigma n} = B^j_{\varphi,l\sigma n}, \quad B^j_{r,l\sigma n} = -E^j_{\varphi,l\sigma n}, \quad (4.5)$$

where

$$y^j_{l\sigma n} \equiv \mathrm{k}^j_{\perp l\sigma n}\rho,\ l = \pm 1, \pm 2 \ldots, \sigma = \pm 1, n = 0, 1, 2 \ldots,$$

and

$$\widetilde{\mathfrak{C}}^j_{l\sigma n} = F^j_{l\sigma n}\big(\xi + \Phi^j_{l\sigma n}(\zeta)\big) \exp\big(-i\Phi^j_{l\sigma n}(\zeta)\big),$$

$$\Phi^j_{l\sigma n}(\zeta) = \frac{1}{2}\int_{\zeta_{j-1}}^{\zeta} (\mathrm{k}^j_{\perp l\sigma n})^2(\zeta')d\zeta' + (\zeta - \zeta_{j-1})\frac{1-\varepsilon_c}{2}, \quad (4.6)$$

are the mode coefficients; $\zeta_j = k_0 z_j$; $\mathrm{k}^j_{\perp l\sigma n}$ are the transverse wave vectors:

$$\mathrm{k}^j_{\perp 0-1n} = (u_{1,n}/\mathscr{R}_j)\left(1 - i\mu_B/\mathscr{R}_j\right),$$
$$\mathrm{k}^j_{\perp 01n} = (u_{1,n}/\mathscr{R}_j)\left(1 - i\mu_E/\mathscr{R}_j\right), \quad (4.7)$$
$$\mathrm{k}^j_{\perp l\sigma n} = (u_{l-\sigma,n}/\mathscr{R}_j)\left(1 - i\mu^+/\mathscr{R}_j\right),$$

$l = \pm 1, \pm 2, \ldots$; $\mathscr{R}_j = k_0 R_j$ and $\mu^\pm \equiv (\mu_E \pm \mu_B)/2$, $\mu_B = 1/\sqrt{\varepsilon_w - 1}$, $\mu_E = \varepsilon_w/\sqrt{\varepsilon_w - 1}$, $u_{l,n}$ is the nth root of the lth order Bessel function, J_l, $J_l(u_{l,n}) = 0$.

Functions $F^j_{l\sigma n}$ are determined by the conditions of continuity of r- and ϕ- components of laser fields at the boundary between jth and $j-1$th intervals as

$$F^j_{l\sigma n}(\xi) = \sum_{n'} F^{j-1}_{l\sigma n'}\big(\xi + \Phi^{j-1}_{l\sigma n'}(\zeta_{j-1})\big) e^{-i\Phi^{j-1}_{l\sigma n'}(\zeta_{j-1})}$$
$$\times \frac{1}{N_{l-\sigma,n}} \int_0^1 y J_{l-\sigma}(u_{l-\sigma,n} y) J_{l-\sigma}\left(u_{l-\sigma,n'} \frac{y R_j}{R_{j-1}}\right) dy, \quad (4.8)$$

where $N_{k,n} = \int_0^1 y J_k^2(u_{k,n} y)dy$; functions $F^1_{l\sigma n}(\xi)$ for the first interval $j = 1$ are equal to

$$F^1_{l\sigma n}(\xi) = F_\parallel(\xi)\mathfrak{C}_{l\sigma n}, \quad (4.9)$$

[1] Below everywhere in equations, the first line is for electric and the second line is for magnetic fields.

https://doi.org/10.1017/S0022377812000736 Published online by Cambridge University Press

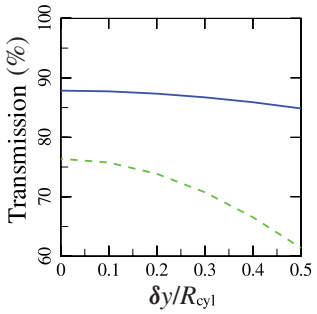


Figure 7. (Colour online) Transmission of laser pulse through the capillary with cylindrical section of length $L_{\rm cyl} = 52$ mm, as a function of relative displacement $\delta_y/R_{\rm cyl}$ of focusing point along OY axis. The laser pulse is incident with the angle $\theta_{\rm inc} = 1$ mrad with respect to the capillary axis OZ, the laser wave vector is in the plane ZOX. Solid line is for the case with cone entrance section with the cone aperture, $R_{\rm cone} = 500$ μm and the length, $L_{\rm cone} = 80$ mm; dashed line is for the case without cone entrance section.

where $F_{\|}(\xi)$ is the longitudinal envelop of the laser pulse before its entrance into the capillary and $\mathfrak{C}_{l\sigma n}$ are coefficients determined by the boundary conditions at the capillary entrance $z = z_0 = 0$ for considered elliptical polarization of incident laser radiation as

$$\mathfrak{C}_{0\sigma n} = -\left[2N_{1,n}\sqrt{1+\eta^2}\right]^{-1} \sum_{k=\pm 1}\left[1+k\eta\right] \times \left[k\tfrac{1-\sigma}{2} + \tfrac{1+\sigma}{2}\right] \mathscr{Z}_{-k,n},$$

$$\mathfrak{C}_{l\sigma n} = \left[2N_{1,n}\sqrt{1+\eta^2}\right]^{-1} (1+\sigma\eta)\, \mathscr{Z}_{l-\sigma,n}, \qquad (4.10)$$

$$\mathscr{Z}_{k,n} = \int_0^1 y F_k(y) J_k(u_{k,n} y) dy,$$

$$F_k(y) = (2\pi)^{-1} \int_0^{2\pi} e^{-ik\varphi} F_\perp(y\mathscr{R}_0, \varphi)\, d\varphi,$$

where $F_\perp(\rho, \phi)$ is the laser pulse transverse envelop at the capillary entrance $z = 0$ and η is the coefficient of polarization ($\eta = 0$ for linear, $\eta = \pm 1$ for circular polarization).

Under the assumption of slowly varying capillary radius and fine capillary segmentation ($z_j - z_{j-1} \ll R_j/(\alpha_j u_{L,N})$, where $\alpha_j = |\partial R/\partial z|_{z=z_{j-1}} \ll 1$, and L, N are the maximum numbers of angular and radial modes under consideration), the above expressions permit one to calculate laser pulse dynamics in capillary waveguide with variable inner radius under conditions close to real experimental ones, when the laser pulse focusing point can be displaced from capillary axis or (and) the laser pulse axis can be non-parallel to the capillary axis, or (and) the laser pulse transverse profile can be with broken cylindrical symmetry (Veysman et al. 2012).

In simulations illustrated in Figs. 7–9, capillaries are composed of two sections: (i) a cone entrance section with length $L_{\rm cone}$ and aperture radius $R_{\rm cone}$, and (ii) a cylindrical section of constant radius $R_{\rm cyl} = 60$ μm and different length $L_{\rm cyl}$. Capillaries are made of glass. Gaussian laser pulses in both radial and time distributions with the waist radius, $r_0 = 60$ μm , and FWHM duration, $\tau_L = 135$ fs, were focused at the beginning of the cylindrical part of capillaries, $z = z_{\rm foc} = L_{\rm cone}$. The laser pulses of wavelength $\lambda_0 = 0.8$ μm were linearly polarized before the capillary entrance. By choosing the laser waist radius r_0 equal to $R_{\rm cyl}$ (in excess of the adjusted spot size $r_0 \cong 0.67\ R_{\rm cyl}$ for the monomode laser propagation in capillary) we model a propagation in capillaries of laser pulses with wide radial wings (Andreev et al. 2008).

Figure 7 illustrates the advantage of use of capillaries with cone entrance section, which can increase considerably the transmission of laser pulse through a capillary in the case of non-perfect focusing and violated coupling conditions. In addition, the cone entrance section permits one to decrease considerably a possible ablation of the capillary entrance face (Veysman et al. 2012).

Figure 8 shows typical space (x, y) and time (ξ) distributions of the laser pulse intensity at different lengths of the laser pulse propagation in capillary waveguide with cone entrance section ($R_{\rm cone} = 100$ μm , $L_{\rm cone} = 20$ mm, and cylindrical section with $L_{\rm cyl} = 40$ mm) and different angles of the laser incidence: $\theta = 1$ mrad (Figs. 8(a) and (b)) and $\theta = 5$ mrad (Figs. 8(c) and (d)). As is seen in Fig. 8, the laser pulse undergoes strong oscillations in longitudinal (with respect to the capillary axis OZ) and transverse directions, which are especially pronounced at the periphery of the pulse. The longitudinal (along ξ coordinate) oscillations will have no considerable effect on the structure of wakefields behind the laser pulse and hence on the acceleration of electrons in these wakefields as long as wakefield amplitude is determined by the integral of the laser field intensity over ξ (Gorbunov and Kirsanov 1987; Esarey et al. 1996). But transverse structure of the laser pulse and wakefields has considerable influence on the effectiveness of electron acceleration and on the quality of accelerated electron bunch (its energy spread, charge, and emittance). It is seen from Fig. 8 that already at small non-zero angle of incidence, $\theta_{\rm inc} = 5$ mrad, the laser pulse is split on separate spots (speckles) (see also Veysman et al. 2010). This structure is absolutely inapplicable for electron acceleration due to strong, varying with propagation, distance z, transverse gradients of the laser pulse intensity, and so wakefields, near the capillary axis. In order to avoid a speckle structure and strong transverse gradients of the fields, one has to ensure the laser angle of incidence $\theta_{\rm inc}$ is no more than 1 mrad (under considered range of parameters, i.e. for a cylindrical part of the capillary with inner radius of the order of tens of microns).

One can also see from Fig. 8 that small-scale transverse and longitudinal oscillations of the laser pulse intensity are maximal near the beginning of the cylindrical part of the capillary (for considered case when the focusing plane, $z_{\rm foc}$, coincides with the end of cone entrance part) and these oscillations decrease with increasing of the propagation distance. This behavior is stipulated by the fact that the laser pulse begins to 'touch' inner walls of the capillary near the point, $z = z_{\rm foc} = L_{\rm cone}$, and high-order radial and angular modes are generated near

https://doi.org/10.1017/S0022377812000736 Published online by Cambridge University Press

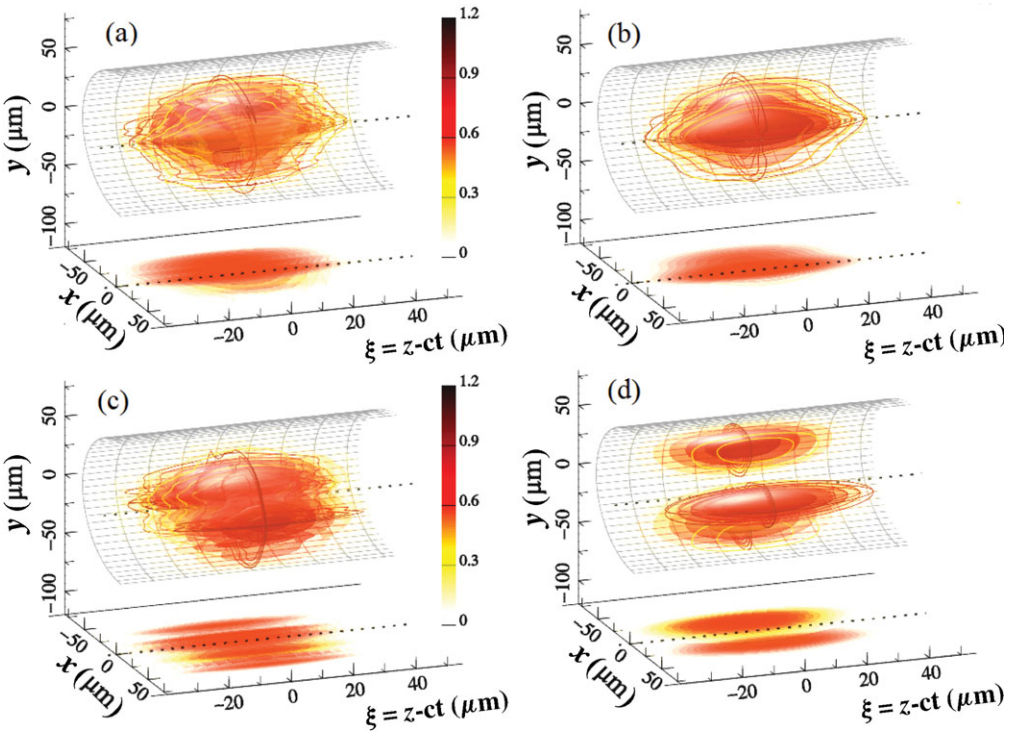


Figure 8. (Colour online) Intensity distribution in x, y, and ξ coordinates (normalized to the laser pulse maximum intensity at the focus plane, I_L) for the laser pulses propagation in a capillary waveguide with cone entrance section with $R_{cone} =$ 100 μm, $L_{cone} = 20$ mm, and cylindrical section with $L_{cyl} = 40$ mm: (a) and (c) for propagation length, $z = 22$ mm; (b) and (d) for propagation length, $z = 60$ mm; (a) and (b) for the angle of incidence, $\theta_{inc} = 1$ mrad; (c) and (d) for the angle of incidence, $\theta_{inc} = 5$ mrad.

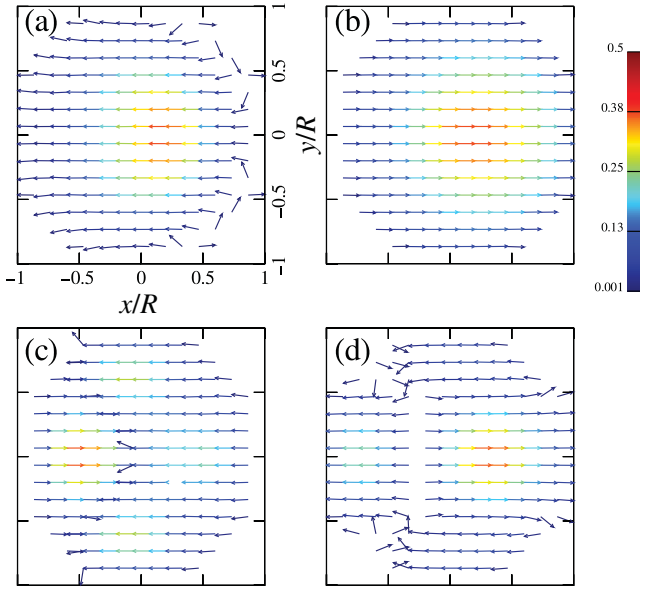


Figure 9. (Colour online) Vector structure of the laser electric field in cross section $\xi = 0$ for the same parameters as in Figs. 8(a)–(d) for the same conditions as in Fig. 8.

this point. In the process of the laser pulse propagation inside the cylindrical part of the capillary, these high-order modes are damped due to energy leakage through capillary walls.

Figure 9 shows the vector structure of the laser electric field in cross section $\xi = 0$ in a capillary waveguide for the same conditions as in Fig. 8. It is seen (Figs. 9(a) and (b)) that in the case of precise enough focusing with $\theta_{inc} \leqslant 1$ mrad laser fields have the same polarization everywhere except for the capillary wall vicinity. Here the polarization deviates from the linear one due to the boundary conditions at the inner surface of the capillary wall manifesting in the first-order terms on the parameter $(k_0 R_{cap})^{-1}$ in the expressions for the radial modes of fields (4.4)–(4.5), and more pronounced for higher modes. At long distances of propagation, high-order modes decay faster than the main mode and therefore changes of polarization near the capillary wall are not so pronounced and are not seen in the scale of Fig. 9(b). For less precise focusing (Figs. 9(c) and (d) at the angle of incidence $\theta_{inc} = 5$ mrad), the laser polarization changes not only near the periphery of the laser pulse but also in the capillary interior, going through zero values of the fields (see Figs. 8(d) and 9(d)). This indicates to the necessity of the vector structure description for the laser field propagating in a capillary with broken symmetry. The respective calculations have shown that redistribution of the laser field vector structure takes place not only for the linear but also for more common case of elliptical polarization of the laser pulse focused into a capillary at broken symmetry.

5. Conclusion

The influence of the nonlinear driving laser pulse dynamics and the electron bunch self-action (plasma lens and

https://doi.org/10.1017/S0022377812000736 Published online by Cambridge University Press

loading effects) to the processes of externally injected electron bunch compression and acceleration in the laser wakefield is analyzed. For considered scheme of electron bunch injection in front of the laser pulse, it is shown that self-consistent 3D electron bunch dynamics can lead to the stronger longitudinal bunch compression than predicted by one-dimensional theory. Obtained modelling results confirm that the nonlinear laser pulse dynamics limits the bunch compression due to variations of phase velocity of the wake. A growth of the injected bunch charge leads to some extent to an increase of the trapped and accelerated bunch charge (together with some growth of the bunch energy spread) and to decrease of the accelerated bunch radius and emittance due to increased bunch self-focusing.

The dynamics of the laser pulse propagation in capillary waveguides under conditions of imperfect focusing is studied. The role of cone entrances to the cylindrical part of a capillary is analyzed and it is demonstrated that matching cones can considerably increase the transmission of laser pulses through the capillary, but cannot mitigate the requirements on the precision of the laser pulse focusing into a capillary. It is shown that even at small, of the order of a few mrad, angles of incidence (i.e. angles between the laser pulse direction of propagation at the capillary entrance and the capillary axis) the laser pulse envelop undergoes pronounced pulsations in longitudinal and transverse directions, which are especially strong near the entrance to the cylinder section of the capillary. It is demonstrated that in this case the transverse distribution of laser fields can have a form of speckles with different polarization of laser field in different spots. This laser intensity distribution reveals strong transverse gradients of the laser, and so wake fields, which can prevent the process of regular electron bunch acceleration. In order to avoid a speckle structure and strong transverse gradients of the fields, one has to ensure that the laser angle of incidence into the capillary does not exceeding 1 mrad (under considered range of parameters, i.e. for a cylindrical part of the capillary with inner radius of the order of tens of microns).

Acknowledgements

This work was supported in part by the Programs on fundamental research of the Russian Academy of Sciences and by the Russian Foundation for Basic Research: Project No. 11-02-12293; CNRS-RFBR PICS project No. 11-02-91058; CNRS-RFBR project No. 10-02-93121, and by the project Triangle de la Physique, RTRA No. 2010-029 T.

References

Abuazoum, S., Wiggins, S. M., Ersfeld, B., Hart, K., Vieux, G., Yang, X., Welsh, G. H., Issac, R. C., Reijnders, M. P., Jones, D. R. et al. 2012 Linearly tapered discharge capillary waveguides as a medium for a laser plasma wakefield accelerator. *Appl. Phys. Lett.* **100**, 014106.

Andreev, N. E., Baranov, V. E., Cros, B., Fortov, V. E., Kuznetsov, S. V., Maynard, G. and Mora, P. 2011a Electron bunch compression and acceleration in laser wakefield. *Nucl. Instrum. Methods Phys. Res.* A **653**, 66 –71.

Andreev, N. E., Cros, B., Maynard, G., Mora, P. and Vojda, F. 2008 Coupling efficiency of intense laser pulses to capillary tubes for laser wakefield acceleration. *IEEE Trans. Plasma Sci.* **36**, 1746–1750.

Andreev, N. E., Gorbunov, L. M., Kirsanov, V. I., Nakajima, K. and Ogata, A. 1997 Structure of the wake field in plasma channels. *Phys. Plasmas* **4**, 1145.

Andreev, N. E., Kirsanov, V. I. and Gorbunov, L. M. 1995 Stimulated processes and self-modulation of a short intense laser pulse in the laser wake-field accelerator. *Phys. Plasmas* **2**, 2573.

Andreev, N. E. and Kuznetsov, S. V. 2003 Guided propagation of short intense laser pulses and electron acceleration. *Plasma Phys. Control. Fusion* **45**(12A), 39.

Andreev, N. E. and Kuznetsov, S. V. 2008 Laser wakefield acceleration of finite charge electron bunches. *IEEE Trans. Plasma Sci.* **36**(4), 1765–1772.

Andreev, N. E., Kuznetsov, S. V., Cros, B., Fortov, V. E., Maynard, G. & Mora, P. 2011b Laser wakefield acceleration of supershort electron bunches in guiding structures. *Plasma Phys. Control. Fusion* **53**, 014001.

Courtois, C., Couairon, A., Cros, B., Marques, J. R. and Matthieussent, G. 2001 Propagation of intense ultrashort laser pulses in a plasma-filled capillary tube: simulations and experiments. *Phys. Plasmas* **8**, 3445.

Esarey, E., Schroeder, C. B. and Leemans, W. P. 2009 Physics of laser-driven plasma-based electron accelerators. *Rev. Mod. Phys.* **81**, 1229–1285.

Esarey, E., Sprangle, P., Krall, J. and Ting, A. 1996 Overview of plasma-based accelerator concepts. *IEEE Trans. Plasma Sci.* **24**, 252–288.

Gorbunov, L. M. and Kirsanov, V. I. 1987 Excitation of plasma-waves by short electromagnetic-wave packets. *Sov. Phys. JETP* **66**, 290–298.

Schroeder, C. B., Benedetti, C., Esarey, E., van Tilborg, J. and Leemans, W. P. 2011 Group velocity and pulse lengthening of mismatched laser pulses in plasma channels. *Phys. Plasmas* **18**, 083103.

Spence, D. J. and Hooker, S. M. 2000 Investigation of a hydrogen plasma waveguide. *Phys. Rev.* E **63**, 015401.

Sprangle, P. and Esarey, E. 1992 Interaction of ultrahigh laser fields with beams and plasmas. *Phys. Fluids* B **4**, 2241.

Tajima, T. and Dawson, J. M. 1979 Laser electron accelerator. *Phys. Rev. Lett.* **43**, 267–270.

Veysman, M., Andreev, N. E., Cassou, K., Ayoul, Y., Maynard, G. and Cros, B. 2010 Theoretical and experimental study of laser beam propagation in capillary tubes for non-symmetrical coupling conditions. *J. Opt. Soc. Am.* B **27**, 1400-1–10.

Veysman, M., Andreev, N. E., Maynard, G. and Cros, B. accepted Non-symmetric laser pulses propagation in capillaries with variable radius. *Phys. Rev.* E.

Wiggins, S. M., Issac, R. C., Welsh, G. H., Brunetti, E., Shanks, R. P., Anania, M. P., Cipiccia, S., Manahan, G. G., Aniculaesei, C., Ersfeld, B. et al. 2010 High quality electron beams from a laser wakefield accelerator. *Plasma Phys. Control. Fusion* **52**, 124032 (8 pp).

https://doi.org/10.1017/S0022377812000736 Published online by Cambridge University Press

Wojda, F., Cassou, K., Genoud, G., Burza, M., Glinec, Y., Lundh, O., Persson, A., Vieux, G., Brunetti, E., Shanks, R. P. et al. 2009 Laser-driven plasma waves in capillary tubes. *Phys. Rev.* E **80**, 066403.

Zigler, A., Ehrlich, Y., Cohen, C., Krall, J. and Sprangle, P. 1996 Optical guiding of high-intensity laser pulses in a long plasma channel formed by a slow capillary discharge. *J. Opt. Soc. Am.* B **13**, 68–71.

https://doi.org/10.1017/S0022377812000736 Published online by Cambridge University Press